IEEE Access
Multidisciplinary | Rapid Review | Open Access Journal

Received December 21, 2020, accepted January 5, 2021, date of publication January 11, 2021, date of current version January 26, 2021.

*Digital Object Identifier 10.1109/ACCESS.2021.3050786*

# Design and Analysis of a Linear Digital Variable Stiffness Actuator

**YAPENG XU, KAI GUO, JIE SUN, AND JIANFENG LI**

Key Laboratory of High Efficiency and Clean Mechanical Manufacture of Ministry of Education, Department of Mechanical Engineering, Shandong University, Jinan 250061, China

Corresponding author: Kai Guo (kaiguo@sdu.edu.cn)

This work was supported in part by the National Natural Science Foundation of China under Grant 51975335, in part by the Key Research and Development Program of Shandong Province (Major Scientific and Technological Innovation Project) under Grant 2019JZZY020318, and in part by the Key Research and Development Program of Shandong Province (Tackling Key Scientific and Technological Problems of Public Welfare) under Grant 2019GGX104008.

**ABSTRACT** In this paper, a novel variable stiffness mechanism (VSM) based on specially designed S-springs made from shape memory alloy (SMA) is developed. Based on the stiffness model, by changing the state combination of the SMA S-springs with different thicknesses, the actuator's stiffness can be discretely adjusted online. The stiffness adjustment range of the actuator can be conveniently extended almost from 0 N/m to infinity by changing the preset spring angle manually offline without a complex mechanical mechanism or replacing any parts. A linear digital variable stiffness actuator (LDVSA) is also designed with the VSM. Some tests of the SMA S-springs, as well as the actuator's stiffness under different configurations, comparisons with other actuators and its trajectory tracking capacity are conducted to verify its design. Then, a dynamic model of the actuator is established and its bandwidth is analysed. Based on this, explosive experiments are designed and performed to explore the application potential of the actuator. Experimental results are provided to illustrate the explosive capacity and energy efficiency of the proposed design.

**INDEX TERMS** Variable stiffness mechanism, flexible actuator, dynamic modeling, shape memory alloy, explosive motion.

## I. INTRODUCTION

Recent years, flexible actuators have received extensive attention due to their superiority in safety, energy efficiency, force sensing, shock absorption and inherent compliance [1]. There are two most popular flexible actuators called series elastic actuator (SEA) and variable stiffness actuator (VSA). Although traditional SEA has the advantages of simplicity, flexibility, easy control and large energy storage capacity [2], [3], the stiffness is difficult to adjust once the design is completed [4], which limits its ability to handle uncertain environments. Unlike SEA, VSA often uses two separate modules with elastic elements to achieve stiffness adjustment and position control [1]. From the principle classification, VSA can be divided into four categories: antagonistic, tunable compliant equilibrium position, lever principle and structure-controlled.

The antagonistic design is inspired by the animal limb movements relying on a pair of actuators to antagonize the joints [5]. Among the actuators with asymmetric antagonism drive, symmetrical parallel mechanism, or the cross coupled configuration [6]–[9], the stiffness adjustment is achieved by antagonistic movement of two motors with nonlinear springs.

To reduce control complexity, the equilibrium position of the elastic elements is utilized. Based on this, MACCEPA tunes the spring pretension through a ball screw mechanism [10], [11]. Another way is to change the effective turns of a linear spring or adjust the angle between the spring deflection direction and the main driving force direction [12], [13]. By adopting a special cam mechanism to regulate the spring balance position, the actuator becomes more compact [14].

There are three key points in a lever that can be employed to change the stiffness: the force action point, the spring action point, and the pivot point [15]. By controlling these three key point's relative positions, the lever arm ratio is adjusted, thereby the stiffness is adapted by changing the transmission ratio between the output side and the elastic elements. In AwAS [16] and HDAU [17], the stiffness is tuned by moving the spring action point while the force action

The associate editor coordinating the review of this manuscript and approving it for publication was Claudia Raibulet.

point and the pivot point are relatively fixed. The approach of stiffness adjustment by changing the pivot point has been sought after by many people for its simplicity. AwAS-II [18] regulates the stiffness continuously from zero to infinity by changing the pivot point with a ball-screw drive. The stiffness adjustment range is hardly affected by the spring's stiffness, and the lever arm is short, which makes the actuator compact and light, and improves the stiffness response speed. Similarly, pVSJ [19] with two custom-made torsional springs also regulates the stiffness by a linear actuator to change the pivot point. However, the pivot is in contact with the springs, and the integration of sensors and transmission mechanisms is poor, which reduces the actuator compactness. The main drive chain is not designed, which makes it just a passive variable stiffness joint. High energy consumption for stiffness adjustment of the two actuators above is required due to the high sliding friction and weight resulted from the intermediate link. As an improvement, TSA [20] reduces the high sliding friction to lower rolling friction by a pair of cam-bearing followers (CBFs), which reduces the energy consumption for adjusting stiffness. Wire-rope drive is used to change the pivot point so that its VSM is compact without the intermediate link, and the problems of backlash, weight and size are optimized. With the help of a novel archimedean spiral relocation mechanism (ASRM), SVSA [21] can change the pivot point only by rotation without a linear actuator, which offers a compact structure and smooth force transmission. A spring shaft that keeps vertical to the output link makes the actuator a large deflection angle.

Based on the theory of material mechanics, the bending stiffness $EI/L$ of a beam can be adjusted by changing its geometric or material parameters [22]. By tuning the effective cross section of the compliant component to change its moment of inertia $I$, the stiffness can be manipulated [23]. Although this way can achieve faster stiffness adjustment, the adjustment range is small, and parasitic deformation will occur if stiffness increases, leading to an increase in the adjustment resistance and reducing the adjustment stability. The beam length $L$ is easy to be adjusted and measured by moving the fixed point of a beam or the force action point [24]–[26], but the leaf spring is often long, which reduces the stiffness adjustment speed and the actuator's compactness. With the development of smart materials, such as SMA, it is feasible to change the elastic modulus $E$ to achieve stiffness variation. [27] proposes a variable stiffness axial strut (VSAS), in which a combination of standard and SMA coiled springs provide load support, and the martensite-austenite transformation drives the stiffness change. The SMA springs are connected in series with the standard compression springs. The actuator stiffness decreases if the SMA springs are heated to the activated state (austenite). It increases to the standard spring's stiffness if the SMA springs are deactivated (martensite). However, the design is only in a concept stage, and the load capacity is small. [28] proposes a compliant mechanism with variable stiffness achieved by two rotary actuators and a spiral SMA spring. Only the linear elastic responses (purely austenite or fixed martensitic state) of the SMA spring are used. If the spring is heated above 70 °C, it is considered activated and in a pure austenite state where its stiffness is about 0.308 N/mm. If the spring temperature is below 30 °C, it is in a fixed martensitic state where the stiffness in its elastic range is only 0.165 N/mm. Its stiffness adjustment range is small, and two motors also increase the complexity (control and compactness) of the actuator. [29] proposes a linear variable stiffness actuator, in which a pair of SMA wires and a compressive spring are configured in parallel. The SMA spring's stiffness is changed by the current supplied to it. The compressive spring is used as a synergistic passive bias for repetitive bidirectional actuation, which increases the strain and range of the stiffness variation. However, the actuator's stiffness and effective stroke are highly affected by the force and displacement generated by the SMA wires, respectively. [30] designed a rotary compliant differential SMA actuator, where two antagonistic SMA wires and a torsion spring are connected in series. Only two terminal conditions (full martensite phase and austenite phase) of the SMA wires are used for stiffness variation. Compared with conventional bias and differential SMA actuators, it achieves a higher response speed and larger output angle. In general, VSA based on SMA wire has a narrow stiffness variation range and small load capacity, and the trade-off between size, weight and energy consumption is difficult. By controlling the voltage of the electro-active materials, thereby changing the activation state of the layered leaf springs, and indirectly adjusting the elastic modulus of the electro-active layer, PVDF-VSJ is developed with one motor and discrete stiffness adjustment capacity [31]. However, its narrow stiffness adjustment range and weak load capacity greatly limit its practicability.

Although many VSAs mentioned above have been successfully implemented, compactness and reliability have been obstacles to their practicality. In many instances where additional mechanical mechanisms such as motors, cams, clutches, gear sets, ball screw with guides, etc. are used to adjust stiffness, this leads not only to longer drive chain (higher friction) and bulky size (higher energy consumption), but exposes the actuator to higher risks of failure (higher cost). However, it is not cost-effective to adjust stiffness continuously in some applications, since the increased weight and stiffness regulation require additional energy consumption [18]. As a compromise, it is promising to configure the actuator stiffness discretely by changing the effective number of springs in a VSA. By connecting springs with different stiffness and electromagnetic clutches to the redundant gears of a gear train, the stiffness of a Binary-Controlled Variable Stiffness Joint (BpVSJ) can be discretely configured [32]. Although the gear trains and clutches make the actuator bulky, its stiffness range has a discrete adjustment potential from 0 Nm/rad to (nearly) infinity, and its adjustment response is fast. The actuator stiffness can also be configured discretely by placing locking mechanisms at different points along an elastic cord to change its effective length, such as passive

Discrete Variable Stiffness Joint (pDVSJ-II) that applied to an elbow exoskeleton [33]. The solenoids and cam mechanisms reduce its compactness, but the energy consumption of the stiffness adjustment is low, and the flexibility of use is strong, which is suitable for rehabilitation training.

In this paper, a novel digital VSA based on specially designed SMA S-springs with different thickness is developed. The actuator stiffness can be changed by two ways: (1) configure the active states of each SMA S-spring by controlling its temperature online, (2) modify the stiffness adjustment range by manually changing the preset spring angle offline. The discrete stiffness can be adjusted linearly or nonlinearly within a certain range through spring thickness relationship and active state configurations. The configuration of the preset spring angle enables the range of actuator stiffness to be broadened from almost 0 N/m to nearly infinity. The proposed VSM is only composed of S-springs with heating wires, which greatly improves the compactness and reduces the complexity of the VSA. In a suitable environment where the temperature is much lower than the deactivation temperature of an SMA S-spring and the stiffness regulation speed is not of first importance, the deactivating process (or cooling process) of an SMA S-spring can proceed naturally without the need for a cooling system, which helps to reduce energy consumption for stiffness regulation.

The rest of this paper is arranged as follows. In section II, the VSM design and its stiffness model with stiffness variation performance analysis are presented. Section III shows the actuator design and its implementation and the thermal characteristics of the SMA S-springs. Some basic performance tests and comparison with other VSAs are provided in Section IV. Section V describes the resulted dynamic model and its analysis. The explosive experiments and experimental results with analysis are presented in Section VI. Finally, conclusions and future work are drawn in section VII.

## II. VARIABLE STIFFNESS MECHANISM DESIGN AND ANALYSIS

### A. WORKING PRINCIPLE OF THE VSM

Fig. 1 depicts the VSM that reciprocates along only the $x$ direction in this study. The driving force on the input frame is transmitted to the output frame in series with the S-springs which pushes it to move along the $x$ direction. To ensure that the actuator stiffness is identical in each motion direction, the S-spring is symmetrical. In this study, except for the different thicknesses $h_i$ of the cantilever parts of different S-springs, the rest of the geometric parameters (width $b_i$, radius $r_i$ and opening angle $\theta_0$), preset spring angle $\theta_i$, and installation orientations are always consistent. Based on the bending stiffness $EI/L$ mentioned above where $I = bh^3/12$ and $L = f(r, \theta_i)$, all of these parameters can be used to change the S-spring's stiffness. The width $b_i$ variation has a linear effect on the bending stiffness, which is not conducive to combining a wide stiffness adjustment range and compact design. The influence of changes in thickness $h_i$,

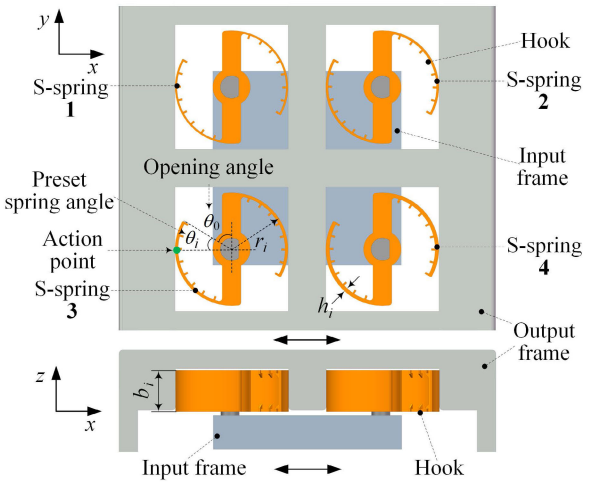


**FIGURE 1. Schematic diagram of the proposed VSM. The VSM reciprocates along only the $x$ direction, and the thickness of the S-springs is different.**

radius $r_i$ and preset spring angle $\theta_i$ on the bending stiffness is non-linear, which is beneficial to design. However, $b_i$, $h_i$ and $r_i$ are difficult to be regulated actively online once the design is completed. Therefore, there are two ways to adjust the actuator stiffness: one is to regulate the preset spring angle $\theta_i$ defined as the corresponding angle between the free end and the action point of the S-spring to change the effective beam length of the S-spring. The other is to control the effective number of springs participating in force transmission because the total stiffness of the VSM is equal to the sum of the stiffness of all S-springs. Although the former can achieve continuous stiffness adjustment by rotating the S-springs synchronously, the transmission and holding mechanisms will reduce the compactness of the actuator. As a compromise between convenience and compactness of stiffness regulation, the second method can be achieved by changing the spring's material properties (here is $E$) online to control whether the S-spring works effectively. Therefore, the S-spring is made of SMA, which can be activated or deactivated with a phase transformation between martensite and austenite by heating it above or below a designable temperature threshold [28].

*Remark 1*: Only two relatively extreme states (martensite and austenite) of the SMA S-springs are used for discrete stiffness regulation in this study. The continuous phase change process (or transient) of the spring material is not considered. The activated or inactivated states of the SMA S-spring are achieved by heating or cooling it after a certain time to the temperature thresholds. For example, if the spring temperature exceeds the heating threshold, it is assumed to be activated and in a pure austenite state. If the spring temperature is lower than the cooling threshold, it is assumed to be inactivated and in a pure martensite state.

As shown in Fig. 2, the states of the corresponding S-springs shown in Fig. 1 are represented by red and blue. Under the same preset spring angle, the stiffness of each

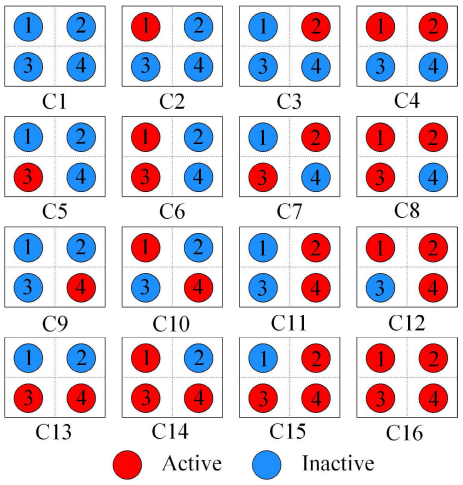


**FIGURE 2.** Digital combination diagram of the VSM under the same preset spring angle where red means active state, and blue represents inactive state.

S-spring is different because of the different thickness that will be explained later. The red indicates that by controlling temperature, the S-spring is in the active state where it shows elastic deformation within the yield stress limit. While, the blue means an inactive state where the S-spring is in martensite phase. Assuming that only pure austenite state or fixed martensitic state of each S-spring is used, such that the states of the SMA S-springs are digital combinations. Inspired by the principle of permutation and combination, by controlling whether the spring is activated, the VSM has $2^4 = 16$ state combinations shown in Fig. 2, which represent 16 discrete stiffness levels under the same preset spring angle.

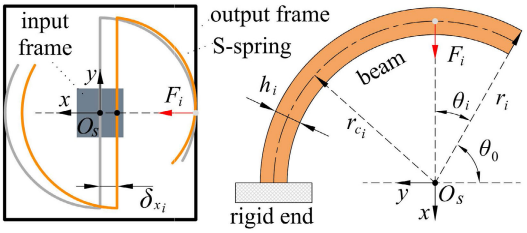


**FIGURE 3.** Force analysis of the proposed SMA S-spring.

### *B. STIFFNESS MODELING AND DESIGN LOGIC*

As illustrated in Fig. 3, there will be a certain deformation $\delta_{x_i}$ between the input frame and the output frame after the $i$th ($i = 1$ to $n$) S-spring is loaded. To simplify the analysis, it is useful to make the following assumptions:

*Assumption 1*: Except for the beam parts of the S-spring, the rest are rigid, and the beam deflection is small compared with its radius and within the elastic range if it is activated.

*Assumption 2*: The force needed for plastic deformation of the S-spring beam under the pure martensitic state is relatively slight, which implies that the residual stiffness can be ignored or regarded almost as 0 N/m.

The beam deflection of the $i$th S-spring under the active state in the $x$ direction is given by [34]

$$\delta_{x_i} = \frac{6F_i r_{c_i}^3}{Eb_i h_i^3}\Omega(\theta_i) = \frac{3F_i(2r_i - h_i)^3}{4Eb_i h_i^3}\Omega(\theta_i) \tag{1}$$

with

$$\Omega(\theta_i) = \pi - (\theta_0 + \theta_i) + \frac{1}{2}\sin\left[2(\theta_0 + \theta_i)\right]. \tag{2}$$

where $r_{c_i}$ is the radius to neutral axis of section.

From the perspective of system force transmission,

$$F_i = K_i \delta_{x_i} \tag{3}$$

where $K_i$ is the stiffness of the $i$th S-spring.

Therefore,

$$K_i = \frac{F_i}{\delta_{x_i}} = \frac{4Eb_i h_i^3}{3(2r_i - h_i)^3\Omega(\theta_i)}. \tag{4}$$

Noting the parallel layout of all S-springs and ignoring the influence of the spring thickness in radial direction ($r_i \gg h_i$), the actuator stiffness can be approximated by

$$K = \sum_{i=1}^{n} K_i s_i \approx \sum_{i=1}^{n} \frac{Eb_i h_i^3 s_i}{6r_i^3\Omega(\theta_i)} \tag{5}$$

and

$$s_i = \begin{cases} 1, & \text{if S-spring } i \text{ is activated} \\ 0, & \text{if S-spring } i \text{ is inactivated} \end{cases} \tag{6}$$

where $n$ is the total number of the S-springs in the VSM, and $s_i$ is the state of the $i$th S-spring.

This study aims to discretely adjust the actuator stiffness by only configuring the state $s$ of the SMA S-springs online, or modify the stiffness adjustment range by manually changing the preset spring angle $\theta$ offline to meet the different applications, and the stiffness regulation speed is not our focus. As shown in Fig. 1, the S-springs are parallel to each other. Thus, the total series stiffness between the input frame and the output frame is equal to the sum of all S-spring's stiffness. Inspired by the algorithm of converting binary numbers to decimal, the state of each S-spring is defined as a Stiffness-Bit whose value can be represented by Eq. (6). To achieve $2^n$ digital-like stiffness variations with $n$ S-springs in parallel, the stiffness of any state combination shown in Fig. 2 under the same preset spring angle must be unique [32]. Therefore, the stiffness of each S-spring under the same state and preset spring angle must meet the following constraints

$$\begin{cases} K_i \neq K_j, & i \neq j \\ K_i + K_j + K_k \neq K_m, & i \neq j \neq k \neq m \end{cases} \tag{7}$$

where $i, j, k, m \in \{1, 2, 3, 4\}$.

Considering the definition of the Stiffness-Bit, the above constraints can be satisfied by the following stiffness relationship of the S-springs under the same preset spring angle

$$K_{i+1} = 2K_i \tag{8}$$

where $i = 1$ to $n - 1$.

**TABLE 1. Nominal parameters of the SMA S-spring.**

| Parameter | Value | Unit |
|---|---|---|
| Spring number $n$ | 4 | - |
| Min. spring thickness $h_1$ | 0.2 | mm |
| Spring width $b$ | 10 | mm |
| Max. spring radius $r$ | 15 | mm |
| Range of the preset spring angle $\theta$ | 120 | ° |
| Spring opening angle $\theta_0$ | 60 | ° |
| Max. allowable deflection $\delta_x$ when $\theta = 0°$ | 8 | mm |
| Max. allowable deflection $\delta_x$ when $\theta = 90°$ | 3 | mm |
| Young's modulus under austenite state $E$ | 75 | GPa |

It can be seen from Eq. (5) that, given the same preset spring angle, spring state and Young's modulus, we have

$$K_{i+1} = \frac{b_{i+1}}{b_i}(\frac{r_i}{r_{i+1}})^3(\frac{h_{i+1}}{h_i})^3 K_i. \tag{9}$$

Obviously, the geometric parameters of the S-spring such as width $b_i$, thickness $h_i$ and radius $r_i$ can be easily designed to satisfy Eq. (8). Considering the compactness of the VSM shown in Fig. 1, we choose the spring thickness $h_i$ as a design parameter, whereas ensure that the radius $r_i$ and width $b_i$ are equal. Then, combining Eq. (8) and Eq. (9), we have

$$h_{i+1} = 2^{\frac{1}{3}} h_i \tag{10}$$

where $i = 1$ to $n - 1$.

Thus, the output force $F$ of the system can be derived as

$$F = \sum_{i=1}^{n} F_i \approx \sum_{i=1}^{n} \frac{Eb_i h_i^3 s_i \delta_{x_i}}{6 r_i^3 \Omega(\theta_i)}. \tag{11}$$

In the above description, $s_i$ is an active online controllable variable that can control each S-spring's state (or $E$ indirectly) for online stiffness adjustment. $\theta_i$ is an active offline controllable variable changed by manually presetting, which can change the stiffness adjustment range of the VSM. The deflection $\delta_{x_i}$ is a passive variable affected by load. The rest of the parameters are spring design constants.

In addition, the strain energy $E_s$ stored in the S-springs of the VSM under the deflection is given by

$$E_s = \sum_{i=1}^{n} \int_0^{\delta_{x_i}} F_i d\delta_{x_i} \approx \sum_{i=1}^{n} \frac{Eb_i h_i^3 s_i \delta_{x_i}^2}{12 r_i^3 \Omega(\theta_i)}. \tag{12}$$

### C. STIFFNESS VARIATION PERFORMANCE ANALYSIS

To analyze the stiffness variation performance of the VSM, the parameters listed in Table 1 are selected. Fig. 4 shows the stiffness variation of the VSM under different spring state combinations depicted in Fig. 2 for different preset spring angles. When $n$ S-springs are all at a same fixed preset spring angle (for example, $\theta = 30$ °), the stiffness changes from combinations C1 to C16 in a linear trend. Although the stiffness is adjusted discretely, this achieves an approximation of the continuously variable stiffness characteristics at a lower cost. Based on Assumption 2, the stiffness under combination C1 can be regarded as 0 N/m. For different preset spring angles, the maximum stiffness of the VSM (appearing at C16) is also different. For example, when the preset spring angle is from 0°, 30° to 60°, the maximum stiffness of the VSM is also from 180 N/m, 2900 N/m to 7200 N/m, which indicates that the stiffness adjustment range of the VSM can be changed by manually presetting the spring angle $\theta$ offline.

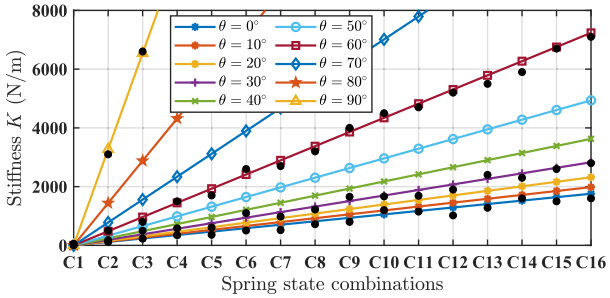


**FIGURE 4. Stiffness variation of the VSM under different spring state combinations with different preset spring angle $\theta$. The black dots represent some measured values.**

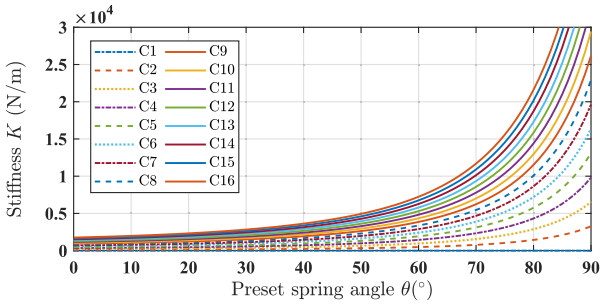


**FIGURE 5. Stiffness variation of the VSM w.r.t the preset spring angle $\theta$ for different state combinations.**

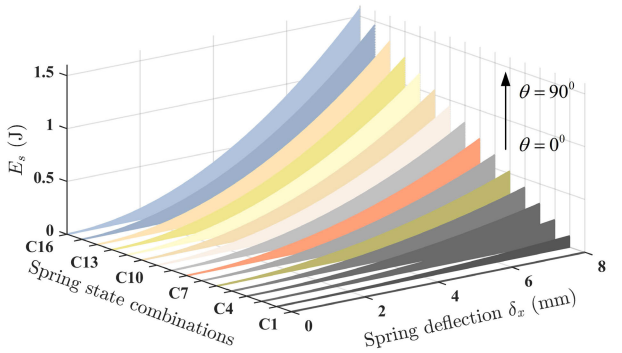


**FIGURE 6. Energy stored in the S-springs of the VSM due to the deflection.**

In addition, except for state combination C1, as shown in Fig. 5, the stiffness of the VSM varies nonlinearly with respect to the preset spring angle $\theta$ (less beam segments), which is beneficial for expanding the stiffness adjustment bandwidth. The elastic energy stored in the S-springs is represented in Fig. 6, which is composed of many sets of curves, where the spring deflection $\delta_x$, spring state combinations and the preset spring angle $\theta$ are the dependent variables.

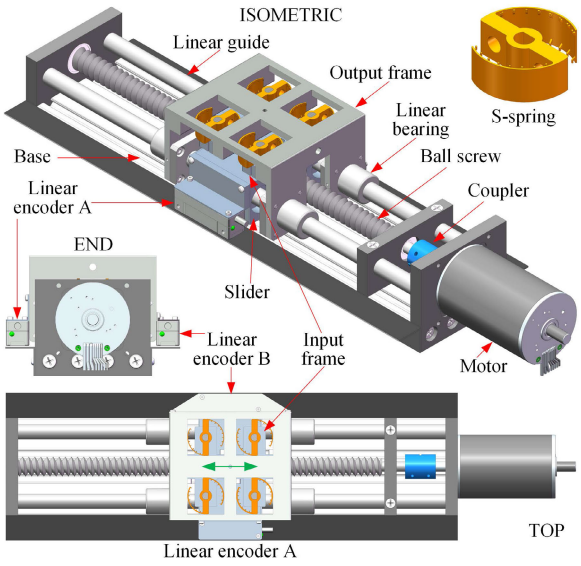


**FIGURE 7.** CAD view of the LDVSA.

According to the design constraints of the allowable deformation, the maximum elastic energy of the VSM is about 0.637 J. The core part of the VSM is a modular unit composed of the S-springs and their base, and its weight is about 0.23 kg. Therefore, the maximum energy density of the VSM is approximately 1880 J/m$^3$, which is beneficial for achieving highly accelerated motion of the output frame.

## III. ACTUATOR DESIGN AND IMPLEMENTATION

### A. MECHANICAL DESIGN

Based on the VSM described above, a LDVSA was designed, as shown in Fig. 7. Due to the compact and modular design of the VSM, it is easily integrated into a conventional linear screw slide table. The input frame on which the S-springs are fixed is installed on a ball screw. The output frame is mounted on symmetrically distributed linear bearings and moves along a linear guide. Moreover, the input frame position and the output frame position are measured by linear encoder A (assembled on the input frame) and linear encoder B (fixed on the output frame), respectively. The deflection $\delta_x$ can be obtained by the position difference of the two encoders relative to a fixed point. Then, combined with the stiffness model, the output force can be estimated based on Hook's law. The motor power is transmitted to the slider through a ball screw with a rigid coupler, part of which is stored in the springs, and the rest is converted into the movement. Fig. 8 shows a schematic diagram of the SMA S-spring unfolded in a plane where an electric heating wire (EHW) is symmetrically wound on the inside of the beams of each S-spring through hooks in a crisscross manner.

### B. IMPLEMENTATION

As shown in Fig. 9, a prototype of the LDVSA is built. The major specifications of the LDVSA are listed in Table 2. A BLDC motor (Maxon, EC-i 52, DC24V) is selected as the power source. Two absolute magnetic linear encoders (Renishaw, LA11SCC13BKA10C) are adopted to measure both the input frame position and the output frame position. A thermocouple is used to measure the spring's temperature to judge whether the spring is activated or deactivated. The preset spring angle $\theta$ is measured by reference lines and tools during the offline manual configuration.

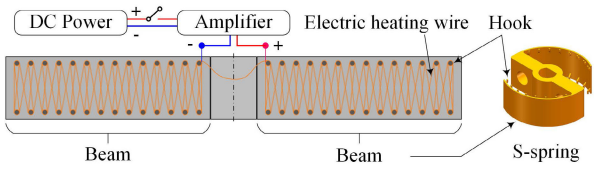


**FIGURE 8.** Diagram of the heating circuit design for the SMA S-spring.

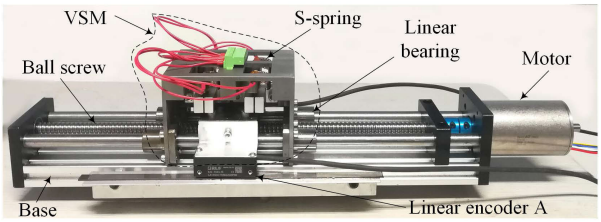


**FIGURE 9.** Prototype of the LDVSA.

**TABLE 2.** Specifications of the actuator prototype.

| Name | Value | Unit |
|---|---|---|
| Size of the VSM | $80 \times 85 \times 50$ | mm |
| Weight of the VSM | 0.23 | kg |
| Motor power | 180 | W |
| Pitch of the ball screw | 2 | mm/rev |
| Nominal output force | $\pm$1295 | N |
| Nominal speed | $\pm$0.15 | m/s |
| Maximum speed | $\pm$0.2 | m/s |
| Effective movement stroke | 200 | mm |
| Position resolution | 0.244 | $\mu$m |

Fig. 10 shows the prototype of the S-springs from the inactive (S1) to active (S6) states by heating simultaneously. The S-springs are made of nickel-titanium (Ni-Ti) alloy by additive manufacturing technology. A set of customized enameled electric heating wires (EEHWs) are wound in the way shown in Fig. 8. The key parameters of the EEHWs are represented in Table 3. Design parameters of the S-springs are the same as in Table 1.

### C. THERMAL CHARACTERISTICS OF THE SMA S-SPRINGS

As shown in Fig. 11, to explore how the spring state would be affected by applying temperature, each S-spring's beam was initially compressed to the same deformation reference point. A thermocouple was attached to the root of the S-spring's cantilever. Then, it was heated from room temperature (about 25 °C) to a degree where it reached another fixed reference point ($r$ mm away from the central axis of the S-spring) with its shape memory property. Finally, the

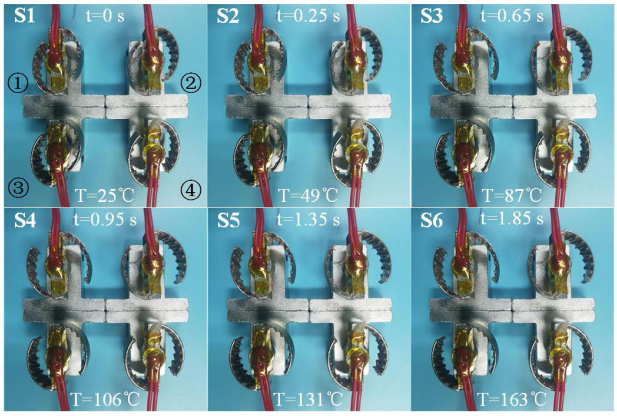


**FIGURE 10.** Prototype and states of the SMA S-springs with the preset spring angle $\theta = 30°$ being heated from room temperature 25 °C (compressed arbitrarily and under inactive state) to over 160 °C (all in active state).

**TABLE 3.** Electrical parameters of the EEHWs on a S-spring prototype.

| Parameter | Value | Unit |
|---|---|---|
| Material | Nichrome | - |
| Nominal heating voltage | 12 | V |
| Nominal heating current | 0.2 | A |
| Melting temperature | 1000 | °C |
| Wire diameter | 0.15 | mm |
| Effective winding turns | 80 | - |
| Effective length | 960 | mm |
| Resistance | 60 | Ω |
| Thermal shock resistance | 3000 | times |

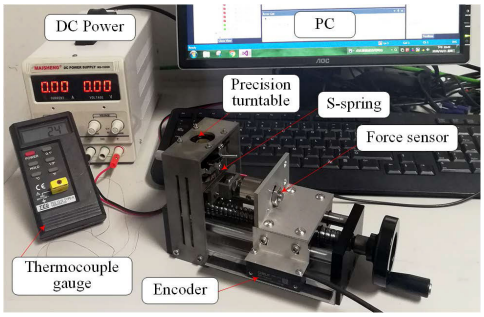


**FIGURE 11.** Experimental platform for the thermal characteristics measurement of the SMA S-springs.

temperature of the S-spring at this time was defined as the activation temperature. The deactivation temperature was defined as the cooling threshold at which S-spring is compressed by $r/2$ mm where the required force is 1/4 of that in the activated state. Besides, as shown in Fig. 12, under the same heating power, the time required for each S-spring to exceed its activation temperature also increases as the thickness increases. During the natural cooling process, the temperature drop process shows a serious nonlinear trend. The time for each S-spring to be cooled to below its deactivation temperature is affected by its thickness the environmental temperature. The states of the S-springs affected by applying

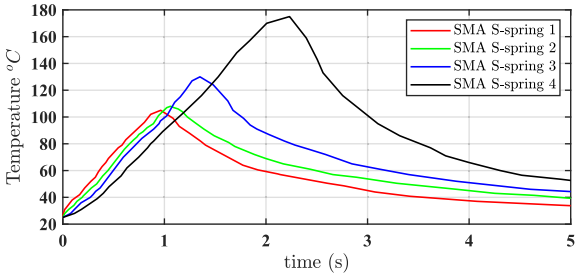


**FIGURE 12.** Temperature vs. time curves of the SMA S-springs from their thermal characteristics experiments.

temperature can also be observed from Fig. 10. Obviously, as the temperature increases, the S-spring 1 is first fully activated (completely restored to the memory shape as S3). If all S-springs are fully activated (as S6), they will keep the memory shape even in the inactivated state and will not deform until they are loaded.

**TABLE 4.** Thermal characteristics of the SMA S-springs.

| Name | S-spring 1 | S-spring 2 | S-spring 3 | S-spring 4 |
|---|---|---|---|---|
| Activation temp. (°C) | > 80 | > 95 | > 125 | > 160 |
| Activation time (s) | 0.63 | 0.94 | 1.27 | 1.84 |
| Deactivation temp. (°C) | < 67 | < 62 | < 56 | < 51 |
| Deactivation time* (s) | 1.7 | 2.5 | 3.4 | 4.9 |

* Measured under the room temperature of 25 °C only with air cooling.

The thermal characteristics of the SMA S-springs without load are listed in Table 4. Obviously, affected by the different beam thicknesses of the S-spring, the temperature thresholds for the state switch of the spring also show similar trend as that of the beam thickness defined in Eq. (10). In addition, the maximum time taken for configuring the stiffness (from C1 to C16) is about 1.84 s. If necessary, the deactivation speed of the S-springs can be accelerated by other cooling methods.

## IV. PERFORMANCE TESTS AND COMPARISON

### A. STIFFNESS VERIFICATION

To evaluate the feasibility of the proposed VSM and the accuracy of the stiffness model, the actual stiffness of the prototype with different preset spring angles were selected as test samples. The output frame was connected to a static force sensor and to push the pulley seat fixed at the end of the LDVSA as shown in Fig. 14. Before the start of each measurement, the input frame was driven by the motor to a reference zero point. After the actuator stiffness was configured, the VSM was loaded and unloaded by controlling the motor's current loop. The linear fitting results were regarded as the obtained stiffness. Some experimental results and theoretical stiffness are exhibited in Fig. 4. The difference between the theoretical and the actual stiffness can be attributed to a certain extent by Assumption 2, which ignores the yield stress in the martensite state of the SMA S-spring. However, from a global perspective, it can be concluded that the actual discrete

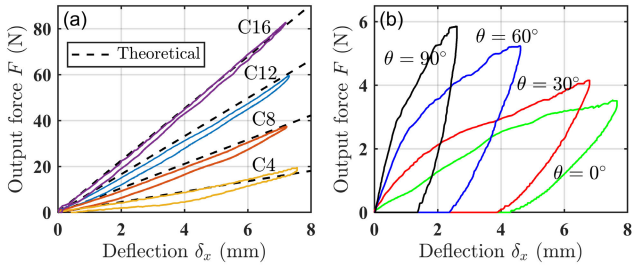


**FIGURE 13.** Theoretical and experimental force-deflection curves of the LDVSA (a) with $\theta = 30°$ (b) under the inactive state with different $\theta$.

stiffness match the theoretical stiffness well, which verifies the stiffness adjustment capacity of the VSM.

As an example, the force-deformation curves of the LDVSA in the active condition when $\theta = 30°$ are shown in Fig. 13(a), which correspond to the stiffness changes of the LD-VSA in the VSA mode in the explosive experiment below. At the beginning, all S-springs are in an uncompressed 'S' shape. In the state combination C4, the force-deformation ex-perimental curve is consistent with the theoretical value ini-tially. The S-springs (1 and 2 under active state) in the VSM show a well elastic deformation trend. As the defor-mation in-creases, the nonlinearity becomes more prominent, which is caused by model assumptions, residual stiffness of S-springs 3 and 4 (under inactive state), and installation error. As the S-spring 3 is activated, the spring state combi-nation becomes C8, the stiffness of the VSM increases, and the linearity of its elastic deformation becomes better. The same conclusion can be obtained from the state combinations C12 and C16. In addition, as the stiffness (slope of the curve) increases, the hysteresis decreases (C4: 21.8%, C8: 16.3%, C12: 11.4%, C16: 8.1%). When all the S-springs are fully activated (C16), the VSM shows better elastic deformation ability.

**TABLE 5.** Deformation parameters of the LDVSA under the inactive state.

| Preset spring angle | $\theta = 0°$ | $\theta = 30°$ | $\theta = 60°$ | $\theta = 90°$ |
|---|---|---|---|---|
| Elastic deformation range (mm) | 0.56 | 0.72 | 0.55 | 0.42 |
| Ratio between the EDR and MD | 0.07 | 0.09 | 0.11 | 0.14 |
| Residual stiffness (N/m) | 582 | 916 | 2148 | 4268 |
| Ratio of RS/MS* | 0.33 | 0.32 | 0.29 | 0.08 |

* Ratio between the residual stiffness and the corresponding maximum stiffness. EDR: elastic deformation range. MD: maximum deformation.

Fig. 13(b) shows the force-deformation curves of the LDVSA when all S-springs are under the inactive state with different preset spring angles. Some relevant deformation parameters of the LDVSA under the inactive state are listed in Table 5. Since the S-springs are not activated (mostly in the martensite phase), after a short linear elastic deforma-tion, the nonlinear plastic deformation of the S-springs is more prominent, and a larger hysteresis loop is also pro-duced. Obviously, the residual stiffness increases as the preset spring angle $\theta$ increases, but the corresponding hysteresis is shrinking.

Although there are different degrees of residual stiffness within the stiffness range determined by each preset spring angle, the elastic deformation range of the S-springs in active state is slight relative to the corresponding maximum defor-mation. This means that once the S-springs are compressed, only a slight deformation can be restored elastically, and there will be a large gap between the input frame and the output frame. At this time, the output frame can be freely moved within a range along the linear guide. Therefore, in this study, the stiffness of the LDVSA at this time is regarded as zero.

It can also be concluded from the curves of C16 in Fig. 13(a) and $\theta = 30°$ in Fig. 13(b) that the stiffness will increase during the heating process under the same preset spring angle, but it will decrease during the cooling process.

*Remark 2*: Under a fixed preset spring angle, the actuator stiffness can be discretely regulated by the state combinations of the SMA S-springs online. The stiffness range can be easily extended almost from 0 N/m to infinity by manually changing the preset spring angle offline without a complex mechanical mechanism or the need to replace new parts.

### B. COMPARISON OF DIFFERENT VSAS

Table 6 provides a comprehensive comparison of the LDVSA with several existing continuous, SMA-based and discrete VSAs (or joints). As shown in Table 6, except for the three VSAs [29], [30] and PVDF-VSJ [31] with extremely small load capacity (MFoT), the actuator volume (size) of the LDVSA (VoA) is the smallest. Although the weight of the LDVSA (WoA) is not competitive, its power-weight ratio (PoA/WoA) is satisfactory, and its weight and volume (size) can be further greatly reduced according to actual stroke and load-bearing requirements. As the core module of a VSA, the proposed VSM has the smallest volume (size) and weight (VoVSM and WoVSM) compared with the continuous VSAs (AwAS-II, SVSA, vsaSDR) and passive discrete actuators (BpVSJ, pDVSJ-II). This is because the driving mechanism of the proposed VSM only consists of some light heating wires instead of complex and heavy mechanical mechanisms, such as screw-slide used in AwAS, grooves with a long drive chain used in SVSA and vsaSDR, clutches and gears used in BpVSJ, solenoids and cams used in pDVSJ-II, etc. The simplification of the proposed VSM not only improves the actuator compactness, but also reduces the energy consump-tion and control cost caused by the weight and friction of the driving mechanism, which improves the reliability of the system. Compared with the VSAs in series configuration such as AwAS-II, SVSA, vsaSDR, etc., the energy density of the proposed VSM (EDrVSM) is relatively high, which helps the output side to achieve greater acceleration. By optimiz-ing the main drive mechanism (stroke, transmission type, etc.) or designing a rotary actuator, the energy density of the LDVSA can be further improved, which contributes to a lightweight application. In addition, the number of actuator (NoA) and other parts of the LDVSA is very few, which is

**TABLE 6. Comparison of the LDVSA with continuous [18], [21], [35], SMA-based [28]–[30] and discrete [31]–[33] VSAs.**

| Name | Stiffness (Nm/rad) | SAT (s) | MEE (J) | VoA ($10^{-3}$m$^3$) | VoVSM ($10^{-3}$m$^3$) | WoA (kg) | WoVSM (kg) | EDrVSM ($10^3$J/m$^3$) | PoA (W) | PoA/WoA (W/kg) | PoVSM (W) | ECoVSM (J) | MFoT (Nm) | NoA / |
|---|---|---|---|---|---|---|---|---|---|---|---|---|---|---|
| AwAS-II [18] | 0-$\infty$ | 2.5 | 5.80 | 3.43 | 1.46 | 1.1 | 0.50* | 3.97 | 56 | 50.91 | 50 | 125 | 80 | $2^b$ |
| SVSA [21] | 1.7-151 | 0.6* | 3.70 | 6.57 | 4.90 | 2.4 | 1.57 | 0.76 | 200 | 83.33 | 40 | 24* | 22.1 | $2^b$ |
| vsaSDR [35] | 127-2095 | 1 | 0.36 | 4.06 | 0.79 | 4 | 1 | 0.46 | 57.2 | 14.30 | 7.2 | 7.5 | 18 | $2^b$ |
| BpVSJ [32] | 0-$\infty$ | 0.035 | 0.71 | 18.41 | 18.41 | 17.9 | 17.90 | 0.04 | / | / | 45 | 1.6 | 12 | $3^d$ |
| pDVSJ-II [33] | 0/2.1/4.1 | 0.04 | <0.64* | 5.48* | 4.54* | 1* | 0.90 | <1.88* | / | / | 163.2 | 6.5 | 3.5 | $4^d$ |
| PVDF-VSJ [31] | <5* | 10* | $\ll$0.64* | 2.88* | 1.60* | 0.4* | 0.10* | $\ll$1.88* | 5 | 12.5* | 1* | 10* | 0.0025 | $1^b$ |
| [28] | 165-308$^a$ | >2* | / | 11.26 | 11.26 | 2* | 0.15* | / | 60 | 30* | 72 | 144* | 3* N | $2^b$ |
| [29] | 3000-3800$^a$ | >1.5* | / | 0.08* | 0.08* | 0.1* | 0.08* | / | 0.4 | 4* | 3.5 | 5.3* | 3.21 N | $2^c$ |
| [30] | 806-10384$^a$ | >10* | / | 0.72* | 0.22* | 0.2* | 0.10* | / | 0.4 | 2* | 2.6* | 26* | 0.03 | $2^c$ |
| **LDVSA** | 0-$\infty^a$ | >1.84 | 0.64 | 3.32 | 0.34 | 3.1 | 0.23 | 1.88 | 180 | 58.06 | 9.6 | 7.9 | 3500 N | $1^b$ |

* Values estimated from literatures. *a*: linear stiffness (N/m), *b*: motor, *c*: SMA wire, *d*: electromagnet. SAT: stiffness adjustment time, MEE: maximum elastic energy, VoA: volume of the actuator, VoVSM: volume of the VSM, WoA: weight of the actuator, WoVSM: weight of the VSM, EDrVSM: energy density relative to the VSM, PoA: power of the actuator, PoA/WoA: power-weight ratio of the actuator, PoVSM: power of the VSM, ECoVSM: energy consumption of the VSM from minimum to maximum stiffness, MFoT: maximum force or torque, NoA: number of actuator.

also very beneficial to the reliability of the system. Therefore, the compactness and reliability of the LDVSA are proved.

Although the above three continuous VSAs can achieve continuous and rapid stiffness adjustment, and hardly consume energy to maintain the stiffness with non-backdrivable mechanisms, they often require 2 motors (NoA) and additional transmission mechanisms, which increases the weight and energy consumption if applied to a robot. Besides, in some robot applications where energy efficiency is required or stiff-ness changing is slow, continuous stiffness variation tracking will lead to an increase in total energy consumption [18].

Therefore, it is meaningful to adjust the stiffness discretely. Although BpVSJ and pDVSJ-II can achieve discrete stiffness configuration rapidly, the sacrifice of compactness is great, and they are only passive VSAs, which will greatly limit their application. Compared with BpVSJ, the weight and volume of the LDVSA are reduced by about 83% and 82%, respectively. The stiffness adjustment range and maximum output force/torque of the LDVSA are much larger than pDVSJ, and its volume is reduced by 40% than that of pDVSJ. Except for PoVSM and WoA, the other parameters of PVDF-VSJ are far inferior to that of the LDVSA. The power of the VSM (PoVSM) of the LDVSA is much lower than that of AwAS-II (81% less), SVSA (76% less) and SMA-based [28] (87% less). The energy consumption of the VSM of the LDVSA is also much lower than that of AwAS-II (94% less), SVSA (67% less) and SMA-based [28] (95% less). These comparisons mean that the LDVSA achieves a good trade-off between energy consumption (low PoVSM and ECoVSM) and compactness (high PoA/WoA and few parts).

Due to the remarkable properties of SMA such as high force-weight ratio, high strain capability, corrosion resistance, light weight, silent, compact and simple design, a passive bias type SMA-based VSA [29] and an active differential bias type SMA-based VSA [30] use SMA wires to achieve both stiffness and output side adjustments with small volume and weight. However, the narrow stiffness adjustment range, unidirectional actuation, and small load capacity of the SMA wires severely limit their practicality. Even if the SMA wire is wound into a coil spring and combined with two flexible arms to form a bias type SMA-based VSA [28], its load capacity and stiffness adjustment range are not improved. However, with the help of the state combinations of $n$ SMA S-springs, the discrete stiffness adjustment range and load capacity of the LDVSA are much larger than that of pDVSJ-II, PVDF-VSJ and the above three SMA-based VSAs.

In general, the outstanding advantages of the LDVSA are: (1) a relatively compact structure and high reliability with very few parts to achieve a wide range of discrete stiffness adjustment; (2) a competitive power-weight ratio (PoA/WoA) with a lot of room for improvement; (3) a good compromise between the advantages of SMA and mechanical stiffness adjustment method (improved discrete stiffness adjustment method and load capacity with a compact structure and low energy consumption VSM).

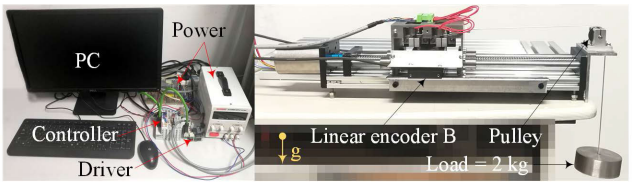


**FIGURE 14. Experimental test bench. (a) Hardware setup. (b) Schematic diagram of the control system.**

### C. TRAJECTORY TRACKING CAPACITY

To explore the performance of the LDVSA in terms of trajectory tracking under different load and stiffness conditions, a series of trajectory tracking experiments were conducted. Fig. 14 depicts the experimental setup where a servo driver (Maxon, EPOS4-50/8) is used to control the motor. The current flowing to the VSM is distributed by relay modules.

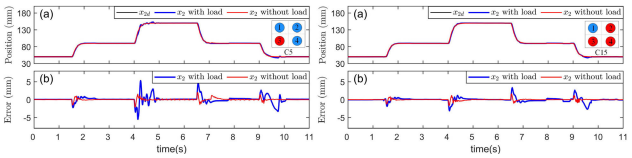

**FIGURE 15.** Ladder step tracking under the low stiffness level of C5 (left) and high stiffness level C15 (right) with $\theta = 60°$.

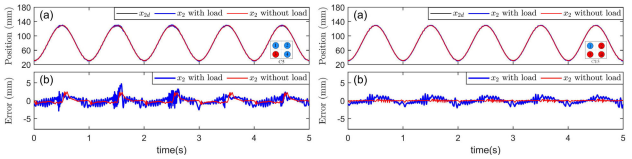

**FIGURE 16.** Sinusoidal trajectory (1 Hz) tracking under the low stiffness level of C5 (left) and high stiffness level C15 (right) with $\theta = 60°$.

The command flows are given by Matlab/xPC. Both the program scanning and sampling rates are set to 1 kHz.

Fig. 15 and Fig. 16 show the trajectory tracking results of the LDVSA with two stiffness configurations under a preset spring angle of $\theta = 60°$ and different load conditions. As expected, the tracking accuracy deteriorates somewhat when the load is added or the stiffness decreased. However, on the whole, during the step response process or the sinusoidal trajectory tracking process, the maximum tracking error is always less than 7 mm, which verifies the effectiveness of the designed LDVSA. Moreover, the tracking capacity under low stiffness and/or heavy load conditions can be further improved by advanced control algorithms.

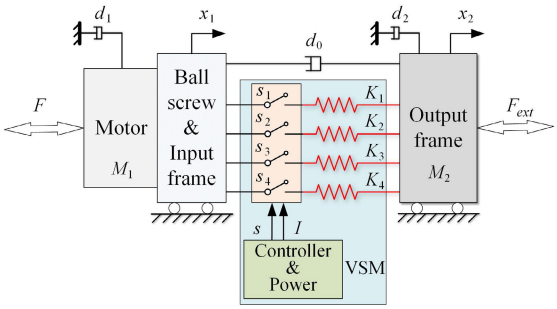


**FIGURE 17.** Modeling of the LDVSA in translational motion.

## V. DYNAMIC MODELING

To analysis the bandwidth and impedance range of the actuator, it is necessary to model its dynamics. As shown in Fig. 17, the LDVSA is considered as a system contains only translational parts by converting the rotary parts to equivalent translational parts. Based on Assumption 1, the actuator's dynamic according to Newton's second law is [36], [37]

$$\begin{aligned} M_1\ddot{x}_1 &= F - K(x_1 - x_2) - d_1\dot{x}_1 - d_0(\dot{x}_1 - \dot{x}_2) \\ M_2\ddot{x}_2 &= K(x_1 - x_2) + d_0(\dot{x}_1 - \dot{x}_2) - d_2\dot{x}_2 - F_{ext} \end{aligned} \tag{13}$$

with

$$M_1 = J(2\pi/p)^2 + M_{is} \tag{14}$$

where $M_1$ and $J$ are the sum of the equivalent mass and moment of inertia from the motor's rotor to the S-springs and the input frame, respectively; $M_{is}$ is the mass of the input frame with the S-springs, $M_2$ is mass of the output frame, $x_1$ and $x_2$ are the displacements of the input frame and output frame, respectively; $F$ is the driving force, $K$ is the actuator stiffness defined by Eq. 5, $d_0$ is the damping coefficient between the input frame and output frame, $d_1$ and $d_2$ are the damping coefficients of the driving side and the output side, respectively, and $F_{ext}$ represents the external force such as load, disturbance or interaction.

To identify some of the dynamic parameters of the LDVSA, step movement experiments like in Fig. 15 were performed. After configuring the stiffness of the LDVSA, it was regarded as a simple SEA modeled as a well-known two-mass, spring and damping system [38]. Based on the positions of the input frame and the output frame recorded by the two encoders, least squares fitting (with the help of the System Identification Toolbox of MATLAB) was adopted to estimate the dynamic parameters of the model, the results of which were listed in Table 7. A Bode plot of the LDVSA system was also drawn in Fig. 18 for different stiffness combinations (levels) under different preset spring angles. In general, as analyzed in Section 2, the system bandwidth expanded approximately linearly as the stiffness changed linearly. However, it shows non-linearity if the preset spring angle $\theta$ increases, which is similar to the trend illustrated in Fig. 5. Therefore, the actuator stiffness can be configured over a wider range, such that the resonant frequency may fall well within the bandwidth of the drive motor, which may be helpful in saving energy in some applications [39].

**TABLE 7.** Dynamic parameters of the LDVSA.

| Parameter | Value | Unit |
|---|---|---|
| Moment of inertia of rotary parts $J$ | $2.9\times10^{-5}$ | kg·m$^2$ |
| Mass of $M_{is}$ | 0.592 | kg |
| Equivalent mass before the S-springs $M_1$ | 286 | kg |
| Equivalent mass of the output frame $M_2$ | 0.592 | kg |
| Damping coefficient of the driving side $d_1$ | 18.14 | N·s/m |
| Damping coefficient of the output side $d_2$ | 8.85 | N·s/m |
| Damping coefficient between the two sides $d_0$ | 1.33 | N·s/m |

## VI. EXPLOSIVE EXPERIMENTS AND ENERGY EFFICIENCY

It is practical and useful to equip a VSA on a robot to make it capable of performing some explosive tasks, such as hammering, kicking, jumping, etc. Just like the accumulator in a hydraulic system, due to the elastic elements, a VSA can use stored elastic energy to achieve peak velocity output beyond the drive motor itself [1]. However, in some studies, where a VSA was used to perform explosive tasks with a fixed stiffness setting (like a SEA), the advantage of its variable stiffness was not demonstrated [35]. Earlier research also showed that the peak velocity of a VSA can be amplified by starting a task at a lower stiffness and adjusting it to a stiffer

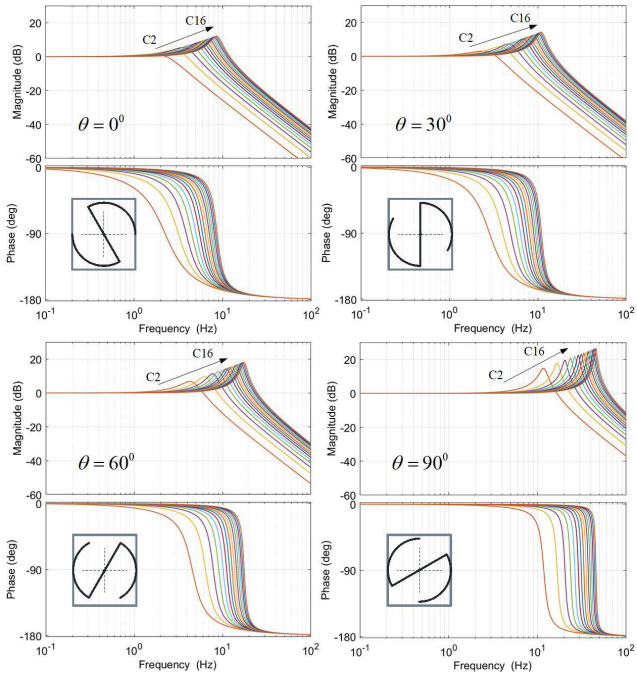


**FIGURE 18.** The bode plot of the LDVSA under different stiffness combinations for the preset spring angles of $\theta = 0°$, $30°$, $60°$ and $90°$.

level during the acceleration phase [40], [41]. Moreover, in this process, changing the stiffness to make the natural frequency $f_n$ of the output side consistent with the track frequency $f_d$ (so-called resonance) not only helps to increase the peak speed, but also minimizes energy consumption [1].

The natural frequency of the LDVSA $f_n$ can be defined as

$$f_n = \frac{1}{2\pi}\sqrt{\frac{K}{M_2}}. \tag{15}$$

### A. EXPERIMENTAL SETUP

From a practical point of view, it is not cost-effective to complete an explosive task using high-frequency motion at the beginning. Therefore, as illustrated in Fig. 19, a 2 kg load was fixed to the output frame so that the natural frequency $f_n$ could be guaranteed within the bandwidth of the drive motor. A 0.18 kg steel ball was placed on the edge of a platform for kicking experiments, and its horizontal distance after being struck was recorded by a ruler and sponge block.

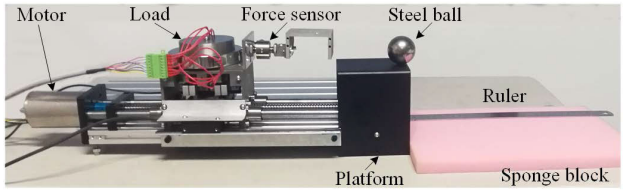


**FIGURE 19.** Test bench setup for the explosive experiments.

To compare the performance of the proposed VSA with the SEA in terms of explosive movement (i.e. kicking ball) and energy efficiency, a trajectory with variable frequency

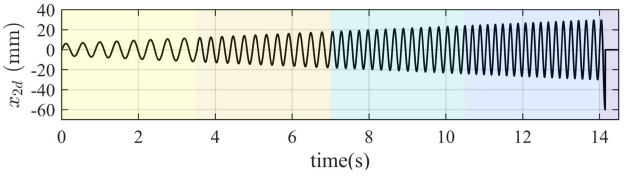


**FIGURE 20.** Task trajectory design for kicking ball experiments.

**TABLE 8.** Experiments design of kicking ball by the LDVSA.

| | | | | | | |
|---|---|---|---|---|---|---|
| | Time $t$ (s) | 0-3.5 | 3.5-7 | 7-10.5 | 10.5-14 | 14-15 |
| Trajectory | Fre. $f_d$ (Hz) | 2.3 | 3.5 | 4.3 | 5.1 | 5.1 |
| | $x_{2d}$ (mm) | $x_{2d} = (24/14t + 6)\sin(2\pi f_d t)$ | | | | |
| VSA* | Spring comb. | C4 | C8 | C12 | C16 | C16 |
| SEA_Low* | Spring comb. | C8 | C8 | C8 | C8 | C8 |
| SEA_High* | Spring comb. | C12 | C12 | C12 | C12 | C12 |
| Rigid | Preset spring angle | $\theta = 120°$ | | | | |

∗ Under the condition that $\theta = 30°$.

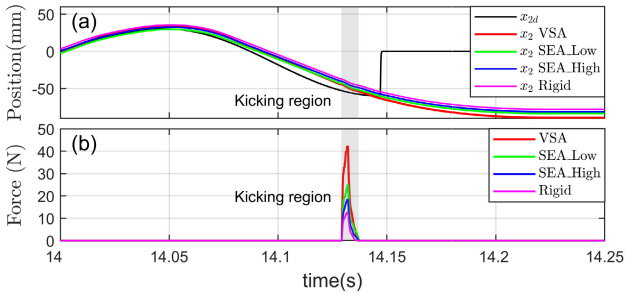


**FIGURE 21.** Kicking experimental results. (a) Output side position. (b) Force.

and amplitude was designed as shown in Fig. 20. As shown in Fig. 2, from states C8 to C12, the S-spring 3 needs to be cooled from above 160 °C to below 60 °C to achieve its deactivation operation. As listed in Table 4, the cooling time of the S-spring 3 under the experimental conditions is about 3.4 s. To ensure that the S-spring has sufficient state switching time during the stiffness adjustment process, and for the sake of simplicity, the time of the four discrete stiffness adjustment processes (C4, C8, C12 and C16) are all set to 3.5 s. Therefore, the total stiffness adjustment time exceeds 14 s, and the explosive movement started after 14 s. However, a simple straight motion for explosive experiment requires the actuator's rapid stiffness adjustment capacity (at the expense of great compactness), which is not in line with our original design intention. Once the trajectory exceeds $-50$ mm, the drive motor will be disabled and the output frame will kick the ball using its stored kinetic energy and elastic energy. As listed in Table 8, during the entire task execution period, different spring combinations (stiffness levels) were tested to make comparisons when the LDVSA is worked as a VSA and an SEA. In addition, by setting the preset spring angle to 120°, it is possible to simulate a nearly rigid actuator.

### B. EXPERIMENTAL RESULTS

The kicking results under four different stiffness configurations (listed in Table 8) are depicted in Fig. 21. The picture

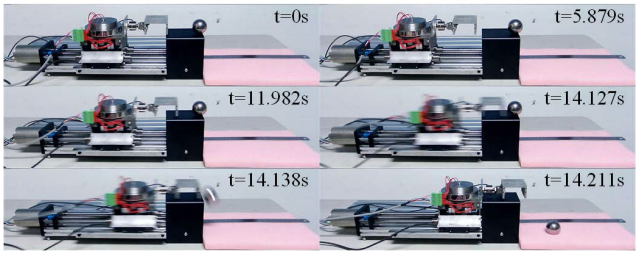


**FIGURE 22.** Pictures of explosive movement at different time instances.

**TABLE 9.** Experimental results of kicking ball by the LDVSA.

| Name | Max. $F$ (N) | Max. $\delta_x$ (mm) | MHDB* (mm) | TAEC* (J) |
|---|---|---|---|---|
| VSA | 42.12 | 7.21 | 101 | 171 |
| SEA_Low | 25.11 | 6.18 | 78 | 194 |
| SEA_High | 18.35 | 3.44 | 64 | 217 |
| Rigid | 12.54 | 0.12 | 51 | 231 |

∗ MHDB: Maximum horizontal distances of the ball. TAEC: Total average energy consumption.

sequence in Fig. 22 shows the motion state of LDVSA at different time instances. Obviously, by changing the natural frequency (adjusting the stiffness) of the LDVSA to make it consistent with the frequency change of the trajectory, and gradually increasing the motion amplitude to accumulate kinetic energy, the explosive power of the actuator with the designed variable stiffness strategy is higher than the other three configurations. The same conclusion can also be drawn from the maximum horizontal distances of the ball (MHDB) listed in Table 9. In addition, regardless of the final kicking action, the entire trajectory can be seen as a cyclic task. In the VSA mode, by adjusting the actuator's stiffness for each task stage, the natural frequency of the actuator $f_n$ is close to the task frequency $f_d$ (resonance occurs), which results in the smallest total average energy consumption (TAEC $=$ 171 J) that is reduced by 26% of the rigid mode. This indicates that in some tasks where the stiffness change is slow, the LDVSA with discrete stiffness adjustment still has a good energy-saving potential. This is similar to the idea in [18] that they only adjust the stiffness of AwAS-II to the average stiffness of each stance phase when utilizing the prosthesis to track a gait trajectory to achieve the minimum stiffness adjustment energy consumption. Considering the compactness of the proposed VSM, the overall energy efficiency of the system will be more competitive if it is applied to a mobile robot for some cyclic tasks, which will be further studied in a future 2-DOF robot to perform some practical tasks such as kicking for repair or hammering-a-nail. The experimental results indicate that the VSA is superior to a SEA or a traditional rigid transmission actuator for similar tasks.

## VII. CONCLUSION

A novel VSM based on specially designed SMA S-springs with different thickness was presented in this paper. Based on the VSM, a LDVSA was developed. By controlling the temperature of the SMA S-springs with heating wires for different states switching, the actuator stiffness could be discretely configured online. Its stiffness range could be expanded from almost 0 N/m to infinity by changing the preset spring angle manually offline without replacing any parts. Comparative discussions verified that the LDVSA was a compact, easy and energy-saving design, that allowed for independent discrete stiffness regulation, since it did not require other complicated mechanical mechanisms. Basic performance tests verified the feasibility of the design. Experimental results of kicking a ball under different stiffness configurations revealed that the LDVSA can be used for some explosive tasks with competitive energy efficiency.

The designed actuator can be used as an end effector for robots to perform special tasks or a joint drive for legged robots. The SMA S-springs can be easily transplanted into a rotary variable stiffness actuator with rotary input frame and output frame. Future work will focus on the development of special robots based on the designed VSM.

## REFERENCES

[1] S. Wolf, G. Grioli, O. Eiberger, W. Friedl, M. Grebenstein, H. Höppner, E. Burdet, D. G. Caldwell, R. Carloni, M. G. Catalano, D. Lefeber, S. Stramigioli, N. Tsagarakis, M. Van Damme, R. Van Ham, B. Vanderborght, L. C. Visser, A. Bicchi, and A. Albu-Schäffer, "Variable stiffness actuators: Review on design and components," *IEEE/ASME Trans. Mechatronics*, vol. 21, no. 5, pp. 2418–2430, Oct. 2016.

[2] Y. Zhao, N. Paine, S. J. Jorgensen, and L. Sentis, "Impedance control and performance measure of series elastic actuators," *IEEE Trans. Ind. Electron.*, vol. 65, no. 3, pp. 2817–2827, Mar. 2018.

[3] H.-C. Hsieh, D.-F. Chen, L. Chien, and C.-C. Lan, "Design of a parallel actuated exoskeleton for adaptive and safe robotic shoulder rehabilitation," *IEEE/ASME Trans. Mechatronics*, vol. 22, no. 5, pp. 2034–2045, Oct. 2017.

[4] S. Li, J. Li, G. Tian, and H. Shang, "Variable stiffness control for SEAs in rehabilitation training," *Adv. Robot.*, vol. 33, nos. 7–8, pp. 424–438, Apr. 2019.

[5] N. L. Tagliamonte, F. Sergi, D. Accoto, G. Carpino, and E. Guglielmelli, "Double actuation architectures for rendering variable impedance in compliant robots: A review," *Mechatronics*, vol. 22, no. 8, pp. 1187–1203, Dec. 2012.

[6] T. Inoue, R. Miyata, and S. Hirai, "Force control on antagonistic twist-drive actuator robot," in *Proc. IEEE/RSJ Int. Conf. Intell. Robots Syst. (IROS)*, Oct. 2016, pp. 3830–3835.

[7] G. Palli, L. Pan, M. Hosseini, L. Moriello, and C. Melchiorri, "Feedback linearization of variable stiffness joints based on twisted string actuators," in *Proc. IEEE Int. Conf. Robot. Autom. (ICRA)*, May 2015, pp. 2742–2747.

[8] Y. Liu, X. Liu, Z. Yuan, and J. Liu, "Design and analysis of spring parallel variable stiffness actuator based on antagonistic principle," *Mechanism Mach. Theory*, vol. 140, pp. 44–58, Oct. 2019.

[9] B. Lukić, K. Jovanović, and T. B. Šekara, "Cascade control of antagonistic VSA—An engineering control approach to a bioinspired robot actuator," *Frontiers Neurorobotics*, vol. 13, pp. 1–15, Sep. 2019.

[10] S. Heins, L. Flynn, J. Geeroms, D. Lefeber, and R. Ronsse, "Torque control of an active elastic transfemoral prosthesis via quasi-static modelling," *Robot. Auto. Syst.*, vol. 107, pp. 100–115, Sep. 2018.

[11] D. Rodriguez-Cianca, M. Weckx, R. Jimenez-Fabian, D. Torricelli, J. Gonzalez-Vargas, M. C. Sanchez-Villamañan, M. Sartori, K. Berns, B. Vanderborght, J. L. Pons, and D. Lefeber, "A variable stiffness actuator module with favorable mass distribution for a bio-inspired biped robot," *Frontiers Neurorobotics*, vol. 13, pp. 1–12, May 2019.

[12] Z. Qaiser, L. Kang, and S. Johnson, "Design of a bioinspired tunable stiffness robotic foot," *Mechanism Mach. Theory*, vol. 110, pp. 1–15, Apr. 2017.

[13] S. Mahboubi, S. Davis, and S. Nefti-Meziani, "Variable stiffness robotic hand for stable grasp and flexible handling," *IEEE Access*, vol. 6, pp. 68195–68209, 2018.

[14] S. Wolf and J.-E. Feenders, "Modeling and benchmarking energy efficiency of variable stiffness actuators on the example of the DLR FSJ," in *Proc. IEEE/RSJ Int. Conf. Intell. Robots Syst. (IROS)*, Oct. 2016, pp. 529–536.
[15] H. Kizilhan, O. Baser, E. Kilic, and N. Ulusoy, "Comparison of controllable transmission ratio type variable stiffness actuator with antagonistic and pre-tension type actuators for the joints exoskeleton robots," in *Proc. 12th Int. Conf. Inf. Control, Autom. Robot.*, 2015, pp. 188–195.
[16] I. Sardellitti, G. A. Medrano-Cerda, N. Tsagarakis, A. Jafari, and D. G. Caldwell, "Gain scheduling control for a class of variable stiffness actuators based on lever mechanisms," *IEEE Trans. Robot.*, vol. 29, no. 3, pp. 791–798, Jun. 2013.
[17] B.-S. Kim and J.-B. Song, "Hybrid dual actuator unit: A design of a variable stiffness actuator based on an adjustable moment arm mechanism," in *Proc. IEEE Int. Conf. Robot. Autom.*, May 2010, pp. 1655–1660.
[18] A. Jafari, N. G. Tsagarakis, I. Sardellitti, and D. G. Caldwell, "A new actuator with adjustable stiffness based on a variable ratio lever mechanism," *IEEE/ASME Trans. Mechatronics*, vol. 19, no. 1, pp. 55–63, Feb. 2014.
[19] M. I. Awad, D. Gan, M. Cempini, M. Cortese, N. Vitiello, J. Dias, P. Dario, and L. Seneviratne, "Modeling, design & characterization of a novel passive variable stiffness joint (pVSJ)," in *Proc. IEEE/RSJ Int. Conf. Intell. Robots Syst. (IROS)*, Oct. 2016, pp. 323–329.
[20] D. Yang, H. Jin, Z. Liu, J. Fan, Y. Zhu, H. Zhang, and H. Dong, "Design and modeling of a torsion spring-based actuator (TSA) with valid straight-arm length adjustable for stiffness regulation," in *Proc. IEEE Int. Conf. Mechatronics Autom.*, Aug. 2016, pp. 2381–2386.
[21] J. Sun, Y. Zhang, C. Zhang, Z. Guo, and X. Xiao, "Mechanical design of a compact serial variable stiffness actuator (SVSA) based on lever mechanism," in *Proc. IEEE Int. Conf. Robot. Autom. (ICRA)*, May 2017, pp. 33–38.
[22] P. Coussot, *Material Mechanics*. Hoboken, NJ, USA: Wiley, Jan. 2005, ch. 1, pp. 4–40.
[23] X. Li, W. Chen, and W. Lin, "Design of a structure-controlled variable stiffness actuator based on rotary flexure hinges," in *Proc. IEEE Int. Conf. Robot. Autom. (ICRA)*, May 2017, pp. 45–50.
[24] W. Wang, X. Fu, Y. Li, and C. Yun, "Design of variable stiffness actuator based on modified Gear–Rack mechanism," *J. Mech. Robot.*, vol. 8, no. 6, Dec. 2016, Art. no. 061008.
[25] Y. Wang and L. Fang, "A simple stiffness equation for a variable stiffness joint using a leaf spring," in *Proc. IEEE Int. Conf. Robot. Biomimetics (ROBIO)*, Dec. 2017, pp. 225–237.
[26] B. J. E. Misgeld, L. Hewing, L. Liu, and S. Leonhardt, "Closed-loop positive real optimal control of variable stiffness actuators," *Control Eng. Pract.*, vol. 82, pp. 142–150, Jan. 2019.
[27] D. J. Siler and K. B. J. Demoret, "Variable stiffness mechanisms with SMA actuators," *Proc. SPIE*, vol. 2721, pp. 427–435, May 1996.
[28] A. Mekaouche, F. Chapelle, and X. Balandraud, "A compliant mechanism with variable stiffness achieved by rotary actuators and shape-memory alloy," *Meccanica*, vol. 53, no. 10, pp. 2555–2571, Aug. 2018.
[29] D. Nalini, D. J. S. Ruth, and K. Dhanalakshmi, "Design of a variable stiffness actuator using shape memory alloy wire," in *Proc. IEEE 7th Power India Int. Conf. (PIICON)*, Nov. 2016, pp. 1–5.
[30] Z. Guo, Y. Pan, L. B. Wee, and H. Yu, "Design and control of a novel compliant differential shape memory alloy actuator," *Sens. Actuators A, Phys.*, vol. 225, pp. 71–80, Apr. 2015.
[31] R. Carloni, V. I. Lapp, A. Cremonese, J. Belcari, and A. Zucchelli, "A variable stiffness joint with electrospun P(VDF-TrFE-CTFE) variable stiffness springs," *IEEE Robot. Autom. Lett.*, vol. 3, no. 2, pp. 973–978, Apr. 2018.
[32] M. I. Awad, D. Gan, I. Hussain, A. Az-Zu'bi, C. Stefanini, K. Khalaf, Y. Zweiri, J. Dias, and L. D. Seneviratne, "Design of a novel passive binary-controlled variable stiffness joint (BpVSJ) towards passive haptic interface application," *IEEE Access*, vol. 6, pp. 63045–63057, 2018.
[33] M. I. Awad, I. Hussain, D. Gan, A. Az-zu'bi, C. Stefanini, K. Khalaf, Y. Zweiri, T. Taha, J. Dias, and L. Seneviratne, "Passive discrete variable stiffness joint (pDVSJ-II): Modeling, design, characterization, and testing toward passive haptic interface," *J. Mech. Robot.*, vol. 11, no. 1, pp. 1–14, Feb. 2019.
[34] B. Richard and J. K. Nisbett, *Shigley's Mechanical Engineering Design*, 10th ed. New York, NY, USA: McGraw-Hill, Jan. 2014.
[35] W. Wang, Y. Zhao, and Y. Li, "Design and dynamic modeling of variable stiffness joint actuator based on archimedes spiral," *IEEE Access*, vol. 6, pp. 43798–43807, 2018.
[36] E. Sariyildiz, G. Chen, and H. Yu, "An acceleration-based robust motion controller design for a novel series elastic actuator," *IEEE Trans. Ind. Electron.*, vol. 63, no. 3, pp. 1900–1910, Mar. 2016.
[37] Y. Park, N. Paine, and S. Oh, "Development of force observer in series elastic actuator for dynamic control," *IEEE Trans. Ind. Electron.*, vol. 65, no. 3, pp. 2398–2407, Mar. 2018.
[38] S. Oh and K. Kong, "High-precision robust force control of a series elastic actuator," *IEEE/ASME Trans. Mechatronics*, vol. 22, no. 1, pp. 71–80, Feb. 2017.
[39] J. Medina, P. Lozano, A. Jardon, and C. Balaguer, "Design and characterization of a novel mechanism of multiple joint stiffness(MMJS)," in *Proc. IEEE/RSJ Int. Conf. Intell. Robots Syst. (IROS)*, Oct. 2016, pp. 2444–2451.
[40] S. Haddadin, M. Weis, A. Albu-Schaeffer, and S. Wolf, "Optimal control for maximizing link velocity of robotic variable stiffness joints," in *Proc. 18th IFAC World Congr.*, vol. 18, no. 1, 2011, pp. 6863–6871.
[41] D. J. Braun, F. Petit, F. Huber, S. Haddadin, P. Van Der Smagt, A. Albu-Schäffer, and S. Vijayakumar, "Robots driven by compliant actuators: Optimal control under actuation constraints," *IEEE Trans. Robot.*, vol. 29, no. 9, pp. 1085–1101, Jul. 2013.

**YAPENG XU** received the B.S. degree in mechanical design and automation engineering from the Inner Mongolia University of Science and Technology, Baotou, China, in 2016, and the M.S. degree in mechanical engineering from Shandong University, Jinan, China, in 2018, where he is currently pursuing the Ph.D. degree.

His current research interests include variable stiffness actuator design, modeling, and control.

**KAI GUO** received the Ph.D. degree in mechanical engineering from Zhejiang University, Hangzhou, China, in 2015.

He is currently an Associate Professor with the Key Laboratory of High Efficiency and Clean Mechanical Manufacture of Ministry of Education, Department of Mechanical Engineering, Shandong University, China. His current research interests include modeling and control of rehabilitation robots and industrial robots, sliding mode control, and other nonlinear control of robotics.

**JIE SUN** received the Ph.D. degree in mechanical engineering from Zhejiang University, Hangzhou, China, in 2004.

He is currently a Professor with the School of Mechanical Engineering, Shandong University, Jinan, China. His research interests include high-speed cutting mechanism of difficult-to-machine materials, deformation control and correction of NC machining of large structure components, intelligent manufacturing, laser processing, and remanufacturing.

**JIANFENG LI** received the Ph.D. degree in mechanical engineering from Shandong University, Jinan, China, in 1994.

He is currently a Professor of mechanical engineering with Shandong University. He has implemented several projects from the National Nature Science Foundation, and two projects from the 973 Program. He has authored or coauthored more than 100 journal and conference papers. His current research interests include advanced design theory as well as nonlinear control theory.